Journal of Alloys and Compounds 807 (2019) 151653

Contents lists available at ScienceDirect

Journal of Alloys and Compounds

journal homepage: http://www.elsevier.com/locate/jalcom

Magnetism and structure in nanocomposite Fe nanoparticle/Al matrix films

M.S. Kurt [a, b, *], S.H. Baker [a], M. Roy [a], M.R. Lees [c]

[a] Department of Physics and Astronomy, University of Leicester, Leicester, LE1 7RH, UK
[b] Department of Fundemantal Science, Erzurum Technical University, Erzurum, Turkey
[c] Department of Physics, The University of Warwick, Coventry, CV4 7AL, UK

ARTICLE INFO

Article history:
Received 6 May 2019
Received in revised form
29 July 2019
Accepted 30 July 2019
Available online 30 July 2019

Keywords:
Fe nanoparticles
Magnetic
Atomic structure
EXAFS

ABSTRACT

We describe magnetometry measurements performed on nanocomposite films formed of Fe nanoparticles embedded in Al matrix. The samples were prepared using a flexible co-deposition technique under Ultra-High Vacuum (UHV) environments. Fe nanoparticles, made by using a gas aggregation source, were co-deposited with an atomic Al beam, made by an MBE source. The Volume Filling Fraction (VFF) of nanoparticles was varied controllably between 4% and 45%, while the mean diameter of Fe nanoparticles produced by the source was ~ 2 nm. Fe K edge extended x-ray absorption fine structure (EXAFS) experiments show that there is a high degree of alloying between Fe nanoparticles and Al atoms. Magnetism in the embedded Fe nanoparticle samples was investigated using a SQUID magnetometer. Atomic moment of Fe in the Fe/Al nanocomposite films increases slightly when the proportion of Fe nanoparticles is increased, but is still significantly lower than the bulk Fe value. In a more detailed analysis, the magnetisation curves were fitted using the Random Anisotropy Model (RAM) which allowed the exchange field and random anisotropy field to be evaluated. The findings and issues raised by this approach are discussed.

1. Introduction

The novel properties of nanoparticles in the nanosize range, which are using as bulding blocks of materials in many area, are hugly important in nanotechnology. This is why in the last few decades this technology has inspired a vast amount of research. Nanoparticles have attracted plenty of interest because of their distinctive novel properties rising from their small size. With decreasing size of nanoparticles for sizes smaller than 10 nm, atom concentiration at the surface layer starts to increase significantly. The atoms located at the surface have a reduced coordination relative to atoms in the bulk; this leads to narrowing effect on the d and f energy bands, which are liable to the magnetisation in rare earth metals and transition metals respectively, giving rise to size-dependent nanoparticle properties [1,2,6]. The size dependency of nanoparticles properties make them different from both the atomic and bulk states. Experimental results from previous research show that both enhancements and reductions in atomic moments have been observed for small enough nanoparticles [1–6]. Permanent ferromagnetic moments have been investigated in nanoparticles that are non-magnetic in bulk form [7].

The atomic structure of embedded nanoparticles is highly critical when determining the magnetic properties of nanoparticles. By changing the atomic structure of embedded nanoparticles, significant changes can be expected in their magnetic propeties, as has been revealed before for Fe and Co nanoparticles [8–21]. One way of achieving this is embedding nanoparticles in a different suitable matrix material systems. To perepare the films of such kind of systems the flexible low energy cluster beam deposition (LECBD) technique [22] can be carried out, where nanoparticles coming from a nanoparticle source and matrix materials coming from a molecular beam epitaxy (MBE) sources are codeposited. Using this technique is highly effective way controling over the atomic structure and volume fraction of the embedded nanoparticles. Atomic structure changes have been observed previously for Fe matrix-embedded Co nanoparticles, where the atomic structure of the Co nanoparticles switched from the hcp to the bcc structure. Higher atomic moments were observed for bcc Co nanoparticles

* Corresponding author. Department of Physics and Astronomy, University of Leicester, Leicester, LE1 7RH, UK.
E-mail address: mustafa.kurt@erzurum.edu.tr (M.S. Kurt).

https://doi.org/10.1016/j.jallcom.2019.151653
0925-8388/

[15]. Another example is that of Fe nanoparticles in an fcc $Cu_{1-x}Au_x$ matrix, in which increasing concentration of Au in the alloy led to a stretching in the Cu—Cu interatomic distance in the alloy matrix and, in turn, led to a stretching in the Fe—Fe interatomic distance in the fcc Fe nanoparticle structure. The structural change in Fe nanoparticles led to a sharp incerease in atomic moment to as high as ~2.5 μ_B/atom which is higher than the bcc bulk Fe value (2.2 μ_B/atom) [20]. Managing magnetic propeties in nanocomposite materials through a highly control on the atomic structure is an important objective for developing new cluster-assembled high performance magnetic devices in many areas, such as magnetic recording [23] and various biomedical application including the treatment of cancer using hyperthermia [24,25].

In this work, we show the results of extended x-ray absorbtion fine structure (EXAFS) and SQUID magnetometry experiments, performed on films consisting of Al matrix-embedded Fe nanoparticles. The nanocomposite thin films were made by the flexible LECBD technique [22]. The structure of atom in the Al-embedded Fe nanoparticles was determined by applying a two shell fit (an Fe—Al shell and an Fe—Fe shell) to the data obtained in the EXAFS experiment, whereas the magnetic moments were obtained from the sample saturation magnetisations measured in the magnetometry measurements. The local magnetic interaction between the embedded Fe nanoparticles was probed using the Random Anisotropy Model (RAM).

2. Experimental details

The LECBD co-deposition technique [22] was used in order to deposit the nanoparticles and matrix materials onto poly-ether-ether-ketone (PEEK) substrates (dimension of 11 mm × 20 mm). Fe nanoparticles and Al matrix material were deposited using a gas aggregation cluster source [26,27] and a molecular beam epitaxy (MBE) source respectively under ultra high vacuum (UHV) environments. The deposition rates of the Fe nanoparticles and Al matrix material were determined using a crystal thickness monitor (XTM); in this way the volume filling fraction (VFF) of embedded nanoparticles in the film could be selected by choosing the appropriate deposition rates. The deposition rate for the Fe nanoparticles was aound 1.5 Å min^{-1} while deposition rates for the Al matrix material varied from about 2 to 25 Å min^{-1}, dependant on the volume filling fraction. The substrate temperature during deposition was 25 °C.

Detailed information relating to the cluster source is described elsewhere [25,27]. Briefly, though, it is a thermal gas aggreagation source that can produce Fe nanoparticles in the size range from 1 to 5 nm with a most probable nanoparticle size at around 2 nm. The nanoparticles are formed by evaporating Fe vapour from a heated crucible into a He background at a pressure of 3 mbar; condensation from the resulting separated vapour leads to the formation of Fe nanoparticles. Differential pumping within the source reduces the background He pressure in the deposition chamber to ~10^{-5} mbar. The base pressure of the system is 2×10^{-10} mbar or better. A quadrupole mass filter, mounted axially within the source, enables nanoparticle sizes to be measured. The size of Fe nanoparticles, with lognormal distribution, produced by the cluster source (when operating under the conditions described above) is shown in Fig. 1.

The samples were made at different volume filling fractions (VFF), from dilute samples to a pure iron nanopartcle film. To investigate the effects of varying the particle-particle interaction, the volume fraction was increased gradually. Before depositing the nanoparticles, a 200 Å film of Ag buffer layer was deposited on the substrate; the films were capped with Ag to avoid oxidation when the films were removed from the deposition chamber.

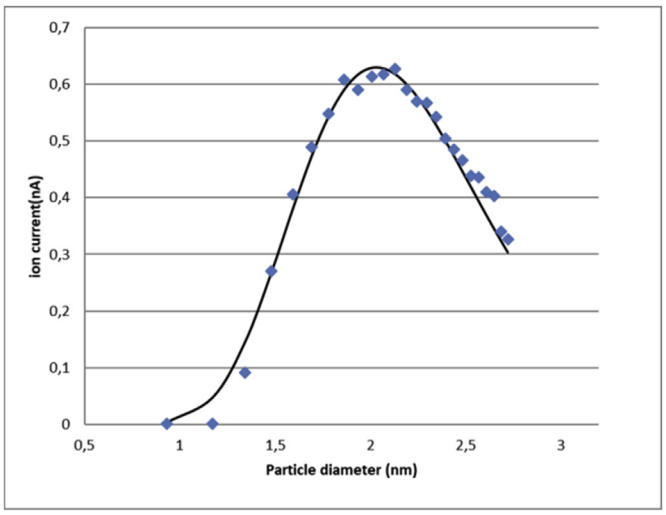

Fig. 1. Size distribution of Fe nanoparticles produced by the cluster source. The line shows a log-normal fit to the data.

The structure of atoms in the Al-embedded Fe nanoparticles has been investigated using Fe K edge EXAFS experiments which was carried out on Beamline B18 at the Diamond Light Source in Oxfordshire, UK. 36-element Ge dedector was used in fluoresence mode to obtained x-ray absorption spectra at room temperature. The double crystal Si(111) monocrhromator is designed to chose the energy of x-rays. The intensity of x-ray was obtained from ionisation chamber, is feded by He gas flow. The EXAFS spectra $\chi(k)$ was provided using the computer program PySpline [28] with measuring background substracted and normalized spectra. Alalysing of these spectra gives details about local environment in structure such as coordinations N_i, interatomic distances r_i and mean square variations in interatomic distance σ_i^2 (Debye—Waller factors). The fast curve wave theory [30] was used to analyse the EXAFS spectra $\chi(k)$ with the EXCURV98 program [29]. The potantials of atomic scattering and shifting in phase were used the Hedin-Lundqvist potentials in program, which are related to the reduction effects on amplitute in EXAFS [31]. All errors are within plus or minus two standard deviations.

Magnetic moment of samples against to applied magnetic field was measured the magnetic field between ±5 T at a 2 K temperature, whereas ZFC and FC graphs were measured the temperature between 2 and 350 K under an applied fixed 0.01 T magnetic field using a SQUID magnetometer. With the total amount of Fe in the samples known, the net atomic moments of each Fe atom could be obtained directly from the sample magnetic moments saturation values. The Random Anisotropy Model (RAM) was applied to investigate the local magnetic interaction between Fe nanoparticles, in Fe nanoparticles embedded in Al matrix films, and also in a film consisting purely of Fe nanoparticles.

3. Results and discussion

3.1. Atomic moments and structure for Fe nanoparticles embedded in an Al matrix

Magnetisation curves measured at 2 K for nanocomposite films with various volume fractions of embedded Fe nanoparticles, and for the pure iron nanoparticle film, are shown in Fig. 2. The same magnetisation curves are shown in Fig. 3 but over a reduced magnetic field range. Hysteresis behaviour is evident in the curves in Fig. 3, which confirms that (at 2 K) the samples behave

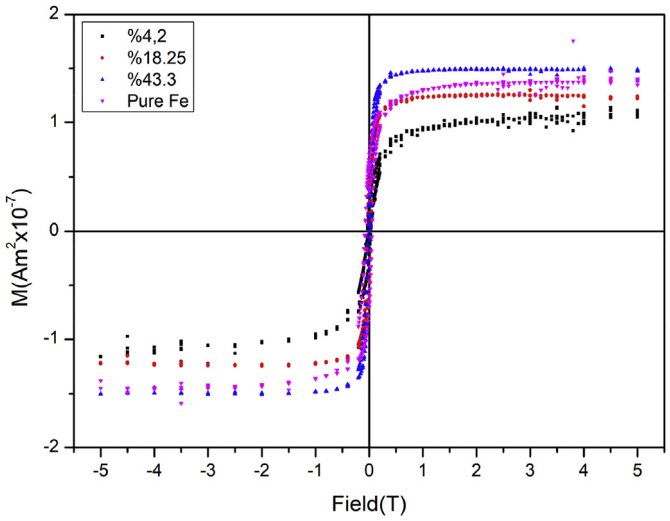

Fig. 2. Magnetisation curves for films of Fe nanoparticles in Al matrices at different volume fraction, and a pure Fe nanoparticles film at 2 K.

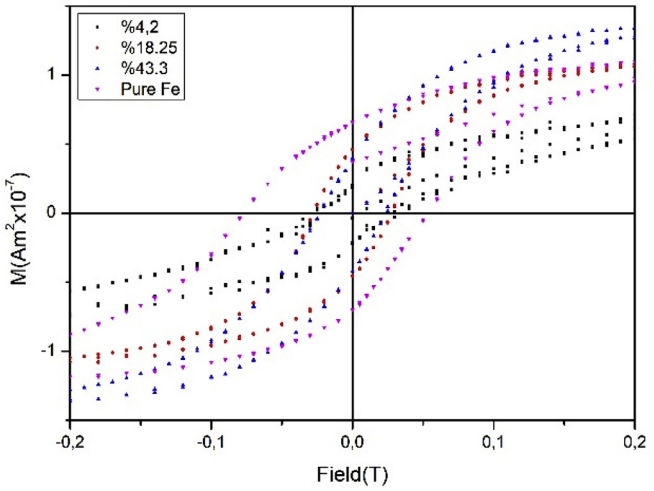

Fig. 3. Magnetisation curves for films of Fe nanoparticles in Al matrices at different volume fraction, and a pure Fe nanoparticles film (magnetic field range between −0.2 and 0.2 T) at 2 K.

ferromagnetically (rather than superparamagnetically). As can be seen from the figure, the coercivities lie in the range 0.02−0.08 T. The magnetic moments of each Fe atom, obtained from the saturation magnetisations, are shown in Fig. 4.

It can be seen from Fig. 4 that the atomic Fe moments in Al-embedded Fe nanoparticles are much less than the value for bulk Fe (2.2 μ_B/atom). The atomic moment for the 4.2% VFF Fe/Al sample, where the nanoparticles are completely isolated from each other, is as low as 0.75 μ_B/atom. It should be noted that the data for the pure Fe nanoparticle film implies an atomic moment around 1 μ_B/atom for this sample. This is at the first slightly puzzling as the atomic moments would be expected to be around the Fe bulk value in a pure Fe nanoparticle film [32]. However there is an exchange bias present in the magnetisation curve for this sample, which implies a degree of oxidation; this would account for a reduction in the atomic Fe moments. No exchange bias effects are present in the data for the films of Fe nanoparticles embedded in Al. So oxidation is not the reason for the low moments seen in these samples.

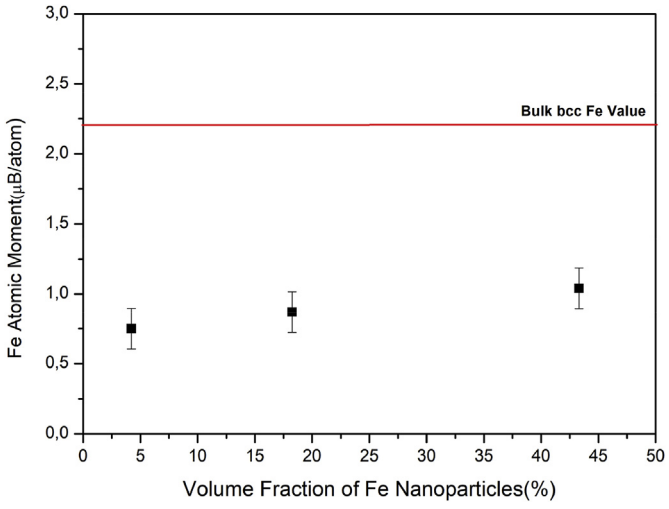

Fig. 4. Magnetic moment per Fe atom value, versus volume filling fraction of Fe nanoparticles in Al.

Reductions in atomic moments of magnetic nanoparticles have been seen previously when the nanoparticles are embedded at dilute VFF in certain matrix materials. A low Fe atomic moment value was observed for embedded Fe nanoparticles at dilute VFF in a Cu matrix by Baker at el [18]. The measured atomic moments had low values between 0.4 and 0.9 μ_B/atom, the reason being a clear structural change in the Cu-embedded Fe nanoparticles from bcc to fcc (of the Cu host) at low filling fractions. Measurements made the temperature at between 2 and 300 K within experimental error, showed the same magnetisations and therefore atomic moments. The observation at 2 K of hysteresis showed that the fcc Fe nanoparticles were magnetic at this temperature, whereas they were found to be superparamagnetic at 300 K. The result showed that the fcc Fe nanoparticles were not antiferromagnetic, unlike previous studies for more fcc Fe precipitates in Cu [33−35]. However a change to fcc is not expected for Fe nanoparticles embedded in Al. Al and Ag both have an fcc structure and very similar lattice parameters (4.05 Å and 4.09 Å respectively). Fe nanoparticles embedded at dilute VFF in Ag have the bulk Fe bcc structure [16] and atomic moment [32]. So (at least in the absence of any other structural changes), an fcc structure is not likely in the Al-embedded Fe nanoparticles.

Co nanoparticles embedded in matrices of Cu and Ag have been observed to have moments very similar to the bulk Co value [36,37]. However, for Mn matrix-embedded Co nanoparticles, the atomic moment per atom is significantly lower than the bulk value [38]; this work report that the Mn-embedded Co nanoparticles had atomic moments that were less than half the bulk Co value (1.7 μ_B/atom). In this case the reason for the reduction of the magnetic moment that was experimentally observed was attributed to considerable alloying between Co and Mn.

In our most recent study; we used the EXAFS measurements to show alloying between the Fe nanoparticles and Al matrix interfaces [50]. Fig. 5(i) and Fig. 5(ii) displays Fe K edge EXAFS (k^3-weighted) and associated Fourier transform for a pure Al matrix-embedded Fe nanoparticles and Fe MBE film respectively. Table 1 shows the fit parameters r_i, $2\sigma_i^2$ and N_i obtained after applying two shell fit (one Fe−Al, one Fe−Fe) to the this data. The fit results for N_i show that each Fe atoms are surrounded by mostly Al atoms rather than Fe. The EXAFS results showed that there are high degree of alloying between the Fe/Al interfaces. Furthermore the alloy structure is consistent within the errors with a bcc FeAl alloy

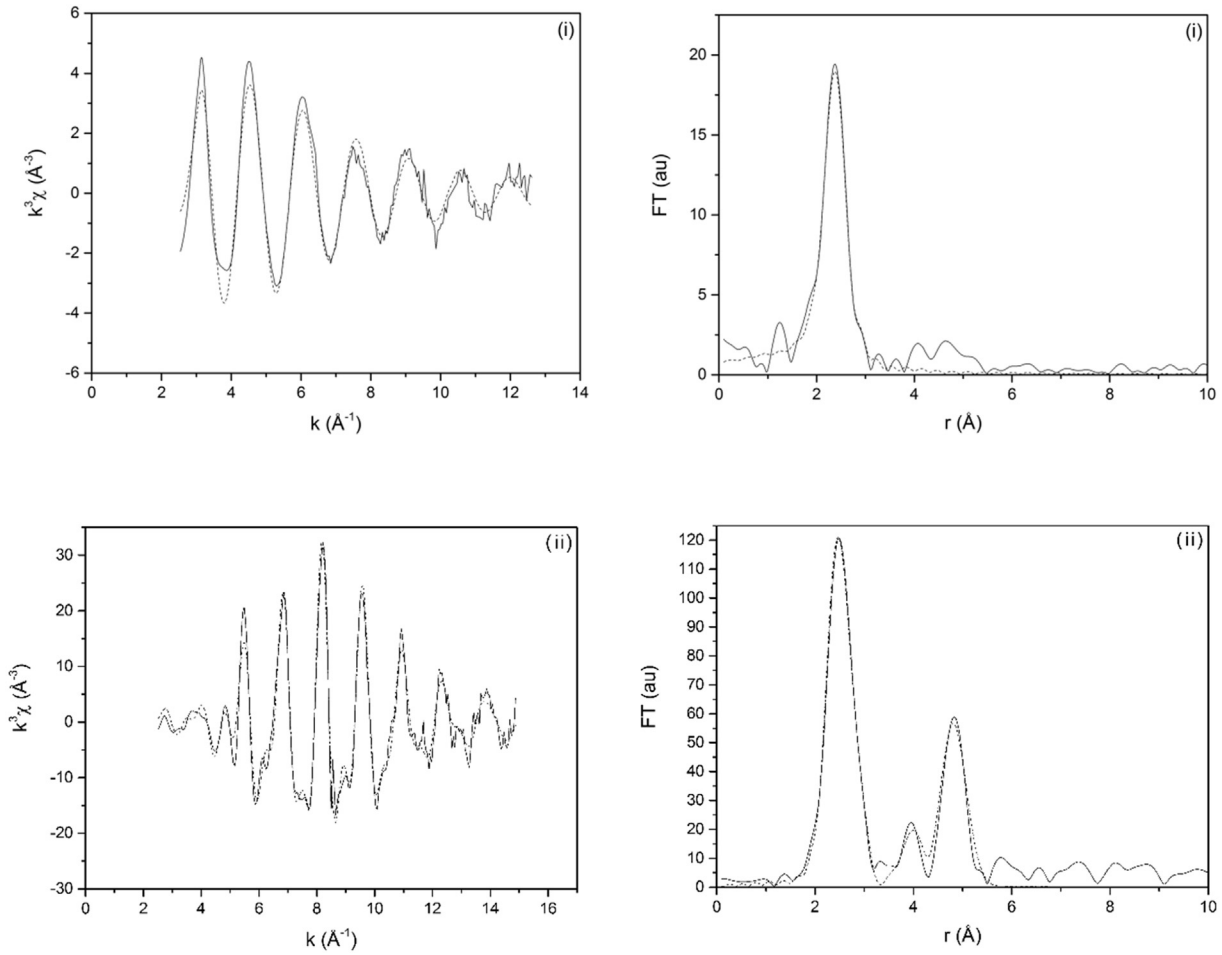

Fig. 5. Fe K edge EXAFS spectrum χ, weighted by k^3, and associated Fourier transform for (i) a Fe nanoparticles embedded in Al with 5.9% VFF film, (ii) an Fe MBE film. The full line represents the data while the dashed line represents the fit to the data. Reproduced with permission from Ref. [50]. Copyright 2019 by the Elsevier.

Table 1
Structural parameters r_i and $2\sigma_i^2$ (interatomic distances and Debye–Waller factors respectively) obtained from fits to the Fe K edge EXAFS spectrum measured for a film of Fe nanoparticles embedded in an Al matrix. Reproduced with permission from Ref. [50]. Copyright 2019 by the Elsevier.

$r_{Fe\text{-}Al} = 2.52 \pm 0.02$ Å
$r_{Fe\text{-}Fe} = 2.55 \pm 0.03$ Å
$2\sigma^2_{Fe-Al} = 0.031 \pm 0.012$ Å^2
$2\sigma^2_{Fe-Fe} = 0.014 \pm 0.010$ Å^2
$N_{Fe-Al} = 6.5 \pm 0.9$
$N_{Fe-Fe} = 0.8 \pm 1.0$

structure, for which low atomic moments have previously been reported [39]. [The results of data analysis for Fe MBE film shows that the film entirely fit to the bcc structure as can be predicted for a Fe film and as reported elsewhere e.g. Ref. [18]].

The low atomic Fe moments measured in the films of Al-embedded Fe nanoparticles are therefore consistent with amount of alloying between the Fe nanoparticles and the Al matrix. As the VFF of Fe nanoparticles in the Al matrix increases, aggregates of nanoparticles become more likely. When the VFF approaches the 3-D percolation threshold of 25%, the number of aggregates will be significant. If large aggregates of nanoparticles are less alloyed than single nanoparticles, the net atomic Fe moment should increase with increasing VFF. As can be seen from Fig. 3, the rise in atomic moment is rather gradual, indicating that the degree of alloying remains significant across the composition range investigated.

3.2. Fitting magnetometry data to the random anisotropy model

The Random Anisotropy Model (RAM) was used to further analyse the magnetic data for Fe nanoparticles embedded in Al. In the last few decades, this model has been developed by various authors [40–42]. In the RAM formalism, the ground state of a magnetic granular film is defined by the relative strength of an RA (random anisotropy) field H_r:

$$H_r = \frac{2K_r}{M_S} \tag{1}$$

and an exchange field H_{ex} :

$$H_{ex} = \frac{2A}{M_S R_a^2} \tag{2}$$

where K_r is the anisotropy of the grain, M_S is the saturation magnetisation, A is the exchange constant for the interaction between the neighbouring particles and R_a is the characteristic grain size for the anisotropy (i.e. the particle size). The relative strength between them is described by the dimensionless ratio:

$$\lambda_r = \frac{H_r}{H_{ex}} = \frac{K_r R_a^2}{A} \quad (3)$$

Although the model has been developed to investigate amorphous, where the randomly oriented anisotropy is determined by local atomic order, it is also a good approach to describe the magnetisation in cluster films [43–45]; the particle size is known so the distance R_a over which anisotropy is correlated is well defined also. Additionally Loffler et al. [46] mentioned that the intra-particle exchange interaction is stronger than the exchange interaction between the particles at the boundaries.

The approach to saturation magnetisation in the measured data is examined in more detail, and compared with the predictions from the random anisotropy model (RAM). As reported by Chudnovsky [47] the approach to saturation is given in three dimensions by

$$M = Ms\left(1 - \frac{1}{30}\frac{\lambda r^2}{\sqrt{h_{ex}}}\int_0^\infty dx C(x) x^2 \exp\left[-x\sqrt{h_{ex}}\right]\right) \quad (4)$$

In equation (4), $h_{ex} = H/H_{ex}$, $\lambda_r = H_r/H_{ex}$ and $C(x)$ is the correlation function describing the distance over which the anisotropy axes are correlated, where $C(0) = 1$ and $C(x = r/R_a > 1) = 0$. For cluster films formed from mono-sized particles, the correlation function can be taken as a step function, with $C(x \le 1) = 1$ and $C(x > 1) = 0$ [45]. Defining parameter p as

$$p^2 = h_{ex}$$

and performing the integration, equation (4) becomes

$$M = M_S\left\{1 - \frac{\lambda r^2}{30p^4}\left[2 - e^{-p}\left(2 + 2p + p^2\right)\right]\right\} \quad (5)$$

This expression was used to fit the approach to saturation magnetisation, measured in the films of Al-embedded Fe nanoparticles as well as the pure Fe nanocluster film. Optimised fits were obtained by means of a spread-sheet programming approach, using the Origin package, with the optimised fit determined from least squares minimisation. The films displayed hysteresis, so the applied field H was replaced by H-H_C in the fits [41]. The fitting procedure allowed us to extract two important parameters. These are the exchange field H_{ex}, related to the local interaction between neighbouring particles, and the other one is the relative strength of the random anisotropy field H_r, related to the internal anisotropy within each particle.

For $\lambda_r > 1$ ($H_r > H_{ex}$), at zero field the magnetic correlation length is equal to R_a, and the each particle magnetic vector is pointed throughout the local intra-particle anisotropy axis. Magnetisation would be same as a spin glass at absolute zero. The magnetic susceptibility would be small in this state, and for a reorientation of the spins of the particles a large magnetic field would be necessary. With increasing particle-particle exchange interaction or decreasing particle-particle anisotropy the magnetic order becomes like correlated spin glass where the magnetic moment of each particles are mostly aligned same direction, however switching direction of magnetic moment alignment along to the system leads to smooth rotation of the magnetisation with a magnetic correlation length which is a factor $1/\lambda_r^2$ larger than the particle size [41]. Therefore when $\lambda_r = 1$, the ground state should in principle change from a spin glass to a correlated super-spin glass. The absolute value of λ_r could be affected by various factors including the angular distribution of the anisotropy axes; Loffler et al. [46] reported that a film produced from nanoclusters with $\lambda_r = 2$ still maintained its correlated super-spin glass state. The nonordered correlated super-spin glass form is fragile and a little amount of applied field produces a ferromagnet with wandering axes [41]. The crossover field is given by $H_{co} = \frac{2A}{M_S R_a^2}$ [49].

Fig. 6 (a)-(d) show the measured approach to saturation at 2 K for all samples, along with the fits to the data. Fig. 6 (e) summarizes how the fit parameters H_{ex} and H_r vary as increased Fe nanoparticle content in the Al matrix. For the pure Fe nanoparticle film, the value for the random anisotropy field H_r is larger than that found previously in Fe nanoparticle films [43]. This could imply a higher value for the anisotropy constant K_r than was measured previously (2.5×10^5 Jm^{-3}) for Fe nanoparticles in Ag [44] (as can be seen from equation (1)). A thin oxide shell around the nanoparticles, consistent with the partial oxidation seen in this sample, would lead to an increased anisotropy. However it should also be noted that partial oxidation would be expected to lead to a lower saturation magnetistion M_s which would also serve to increase H_r. It can also be noted that the exchange field for the film of pure Fe nanoparticle is lower than values measured previously [43]. This is consistent with the exchange as a result of the oxidation on the shell. For the Al-embedded Fe nanoparticles films, the values of H_r and, to a smaller extent, H_{ex} are rather different in the 4.2% VFF film than for the other samples. This is likely due to the fact that the RAM model is not applicable for this dilute sample (where the nanoparticles are well separated), rather than to a significant trend. Moving to the 18.25% VFF film, it can be seen that H_{ex} is low (0.14T), rising slightly as the VFF is increased, towards the value measured in the (partially oxidised) Fe nanoparticle film. From equation (2) it can be seen that H_{ex} is proportional to A (the exchange constant between neighbouring particles), and inversely proportional to M_s (the saturation magnetisation). Since A should scale as M_s^2, H_{ex} should scale with M_s. The trends in H_{ex} with VFF, and atomic Fe moment with VFF (Fig. 2), are similar to one another, which is therefore consistent with the prediction that H_{ex} should scale with M_s. The increase in H_r with VFF is qualitatively similar to that seen for Fe nanoparticles embedded in Co [48].

3.3. Field-cooled and zero-field-cooled magnetic measurements for Al-embedded Fe nanoparticles

The conventional FC (field-cooled) and ZFC (zero-field cooled) curves were obtained with an applied field of 0.01 T for the Fe nanoparticle films in Al. The FC/ZFC magnetisation curves for the 4.2% VFF Fe/Al film are shown in Fig. 7.

The overall form of the curves is characteristic of a superparamagnetic assembly. This relates to a system as reported previously for the dilute film of Fe nanoparticles in a Ag matrix, where magnetic nanoparticles are well separated each other in a non-magnetic matrix [44]. The ZFC curve peak gives an estimated mean blocking temperature. For the temperatures higher than blocking temperature (around 9K), there is not any significant differences were observed between the FC and ZFC curves, as expected by the Langevin function for a uniform applied magnetic field. First separation on the FC/ZFC curves was observed at the blocking temperature where the anisotropy barrier has the highest value. Below the blocking temperature the magnetisation in each nanoparticle becomes frozen along its local anisotropy axis.

For higher volume fraction of nanoparticles, the FC and ZFC data is evidence of interaction between the nanoparticles in the film. As illustrated in Fig. 8, both FC and ZFC curves reach to peak around the 200 K for a sample with 18.25% VFF of nanoparticles. FC curve decreases slightly and makes a pleteau at low temperature, while

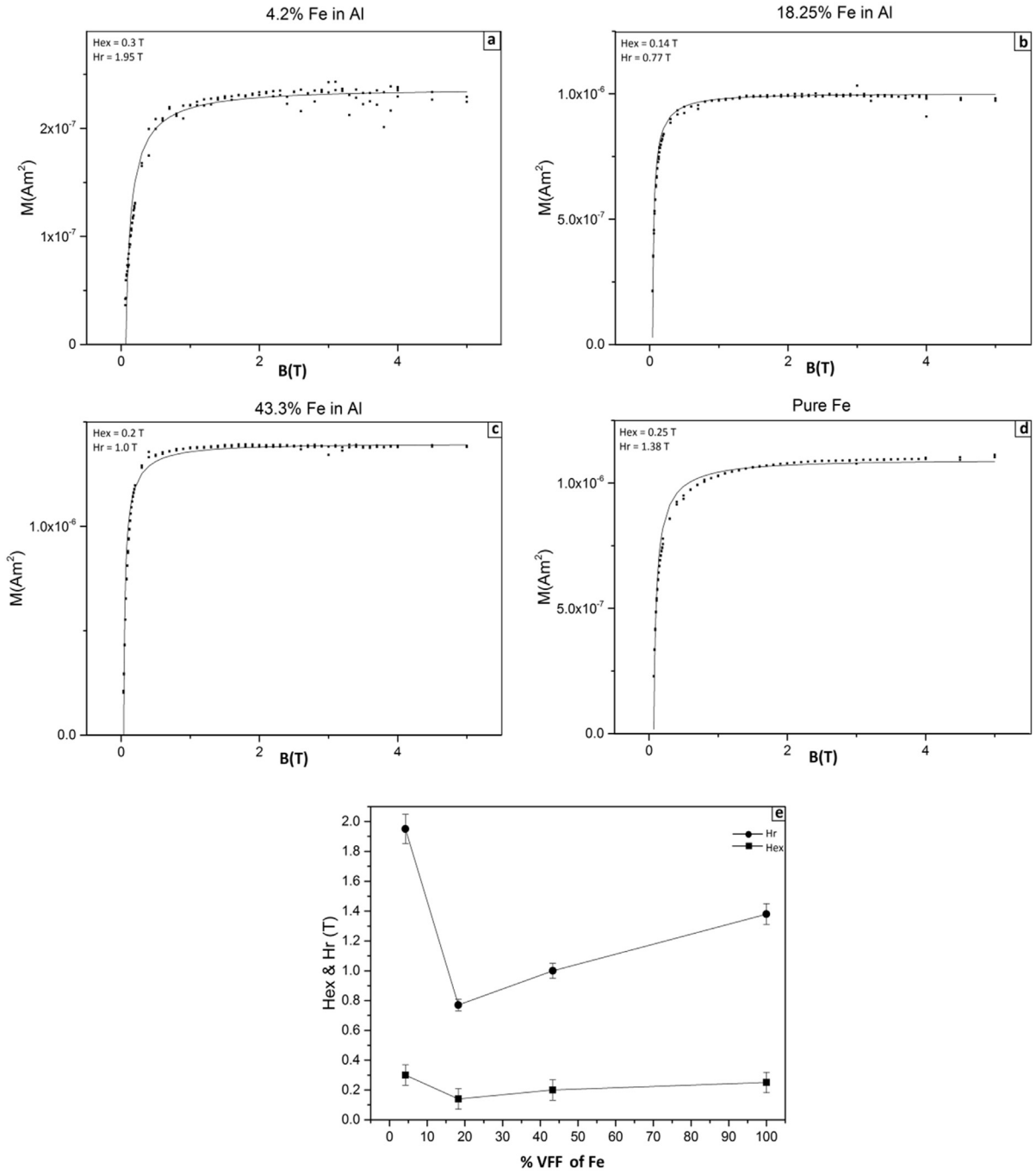

Fig. 6. (a)–(d) Approach to saturation magnetisation of Fe nanoparticles embedded in Al matrices with different volume filling fraction, measured at 2 K. (e) Fitted values of H_r and H_{ex} as a function of Fe VFF.

ZFC curve continuously decreasing. These beheviours are associated with a coordinated freezing of particle moments, and characteristically identical for the spin glass systems. These effects were reported before for Fe nanoparticles in a Ag matrix with higher volume fractions [44]. Also as in this report, we observe an increase in blocking temperature as increased VFF of nanoparticles. According to the authors in Ref. [44], two types of magnetic interaction were required to explain the observed behaviour. The first of these is the exchange interaction between the individual nanoparticle couples into aggregates, allowing to an increase in T_b. The second interaction is a dipolar interaction between aggregates.

4. Conclusions

We have observed that alloying between the Fe nanoparticles and Al matrix leads to the atomic moments of Fe much lower than the bulk Fe value in Al-embedded Fe nanoparticles. The RAM was employed to investigate the local magnetic interaction of Fe nanoparticles. It was found that for pure Fe nanoparticles (albeit partially oxidised) the random anisotropy field H_r has a maximum value and decreases slightly with decreasing volume fraction of Fe for the Fe nanoparticle/Al matrix samples. The exchange field H_{ex} in the Al-embedded Fe nanoparticle samples is lower than for pure Fe,

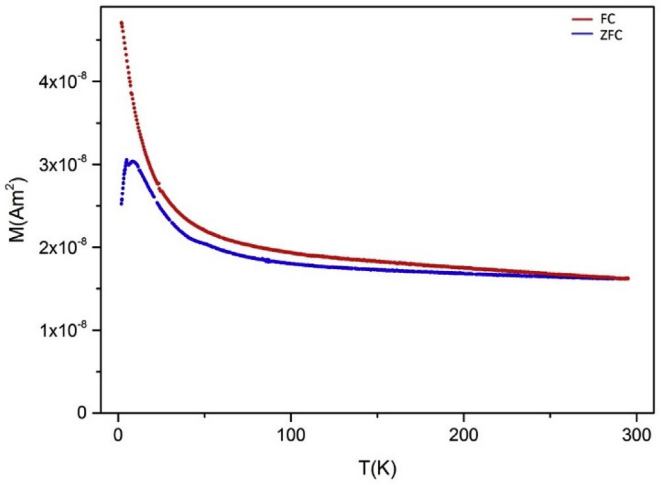

Fig. 7. ZFC and FC magnetisation curves for Fe nanoparticles in Al at a VFF of 4.2%, measured with an applied 0.01 T field.

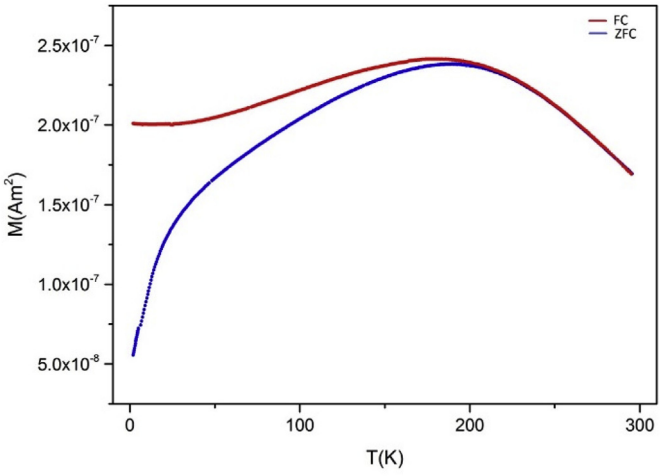

Fig. 8. ZFC and FC magnetisation curves for Fe nanoparticles in Al at a VFF of 18.25% with an applied field of 0.01 T.

although increases slightly with increasing Fe volume fraction. The FC-ZFC magnetisation data for dilute (4.2% VFF) Fe in Al indicates superparamagnetic behaviour. However as increased volume fraction of Fe in Al to 18.25%, the effective blocking temperature increases to a higher value due to magnetic interactions related to a coordinated freezing of particle moments, and spin glass systems.

Acknowledgments

The authors are grateful to Dr Stephen Parry at the Diamond Light Source for his assistance during the EXAFS experiments.

References

[1] I.M.L. Billas, J.A. Becker, A. Châtelain, W.A. de Heer, Phys. Rev. Lett. 71 (1993) 4067.
[2] D.C. Douglass, A.J. Cox, J.P. Bucher, L.A. Bloomfield, Phys. Rev. B 47 (1993) 12874.
[3] S.H. Baker, C. Binns, K.W. Edmonds, M.J. Maher, S.C. Thornton, S. Louch, S.S. Dhesi, J. Magn. Magn. Mater. 247 (2002) 19.
[4] J.T. Lau, A. Fohlisch, R. Nietubye, M. Rief, W. Wurth, Phys. Rev. Lett. 89 (2002), 057201.
[5] J. Bansmann, et al., Surf. Sci. Rep. 56 (2005) 189.
[6] D.C. Douglass, J.P. Bucher, L.A. Bloomfield, Phys. Rev. Lett. 68 (1992) 1774.
[7] A.J. Cox, J.G. Louderback, S.E. Apsel, L.A. Bloomfield, Phys. Rev. B 49 (1994) 12295.
[8] A. García Prieto, M.L. Fdez-Gubieda, A. García-Arribas, J.M. Barandiarán, C. Meneghini, S. Mobilio, J. Magn. Magn. Mater. 221 (2000) 80.
[9] M.P.C. Vergara, J.C. Cezar, H.C.N. Tolentino, M. Knobel, Phys. B 320 (2002) 143.
[10] J.C. Cezar, H.C.N. Tolentino, M. Knobel, Phys. Rev. B 68 (2003), 0544041.
[11] M. Jamet, V. Dupuis, P. Mélinon, G. Guiraud, A. Pérez, W. Wernsdorfer, A. Traverse, B. Baguenard, Phys. Rev. B 62 (2000) 493.
[12] J. Tuaillon, V. Dupuis, P. Mélinon, B. Prével, M. Treilleux, A. Pérez, M. Pellarin, J.L. Vaille, M. Broyer, Philos. Mag. 76 (1997) 493.
[13] V. Dupuis, M. Jamet, L. Favre, J. Tuiallon-Combes, P. Mélinon, A. Pérez, J. Vac. Sci. Technol. A 21 (2003) 1519.
[14] L. Favre, S. Stanescu, V. Dupuis, E. Bernstein, T. Epicier, P. Mélinon, A. Pérez, Appl. Surf. Sci. 226 (2004) 265.
[15] S.H. Baker, M. Roy, S. Louch, C. Binns, J. Phys. Condens. Matter 18 (2006) 2385.
[16] S.H. Baker, M. Roy, S.J. Gurman, S. Louch, A. Bleloch, C. Binns, J. Phys. Condens. Matter 16 (2004) 7813.
[17] M. Sakurai, S. Makhlouf, T. Hihara, K. Sumiyama, K. Wakoh, K. Suzuki, Phys. B 208 (1995) 614.
[18] S.H. Baker, A.M. Asaduzzaman, M. Roy, S.J. Gurman, C. Binns, J.A. Blackman, Y. Xie, Phys. Rev. B 78 (2008), 014422.
[19] S.H. Baker, M. Roy, S.J. Gurman, C. Binns, J. Phys. Condens. Matter 21 (2009) 183002.
[20] S.H. Baker, M. Roy, S.C. Thornton, C. Binns, J. Phys. Condens. Matter 24 (2012) 176001.
[21] S.H. Baker, M. Lees, M. Roy, C. Binns, J. Phys. Condens. Matter 25 (2013) 386004.
[22] A. Pérez, et al., J. Phys. D Appl. Phys. 30 (1997) 709.
[23] V. Skumryev, S. Stoyanov, Y. Zhang, G. Hadjipanayis, D. Givord, J. Nogués, Nature 423 (2003) 850.
[24] Q.A. Pankhurst, N.T.K. Thanh, S.K. Jones, J. Dobson, J. Phys. D Appl. Phys. 42 (2009) 224001.
[25] B. Thiesen, A. Jordan, Int. J. Hyperth. 24 (2008) 467.
[26] S.H. Baker, S.C. Thornton, K.W. Edmonds, M.J. Maher, C. Norris, C. Binns, Rev. Sci. Instrum. 71 (2000) 3178.
[27] G.I. Iles, S.H. Baker, S.C. Thornton, C. Binns, J. Appl. Phys. 105 (2009), 024306.
[28] A. Tenderholt, B. Hedman, K.O. Hodgson, AIP Conference Proceedings 882 (2007) 105.
[29] N. Binsted, EXCURV98, Daresbury Laboratory Computer Program, 1998.
[30] S.J. Gurman, N. Binsted, I. Ross I, J. Phys. C Solid State Phys. 17 (1984) 143.
[31] M. Roy, S.J. Gurman, J. Synchrotron Radiat. 8 (2001) 1095.
[32] C. Binns, M.T. Qureshi, D. Peddis, S.H. Baker, P.B. Howes, A. Boatwright, S.A. Cavill, S.S. Dhesi, L. Lari, R. Kröger, S. Langridge, Nano Lett. 13 (2013) 3334.
[33] S.C. Abrahams, L. Guttman, J.S. Kasper, Phys. Rev. 127 (1962) 2052.
[34] G.J. Johanson, M.B. McGirr, D.A. Wheeler, Phys. Rev. B 1 (1970) 3208.
[35] Y. Tsunoda, S. Imada, N. Kunitomi, J. Phys. F Met. Phys. 18 (1988) 1421.
[36] C. Binns, J. Blackman, Metallic Nanoparticles, vol. 78, Elsevier, Amsterdam, 2009, p. 231.
[37] Y. Xie, J.A. Blackman, Phys. Rev. B 66 (2002) 155417.
[38] C. Binns, N. Domingo, A. Testa, D. Fiorani, K.N. Trohidou, M. Vasilakaki, J.A. Blackman, A.M. Asaduzzaman, S. Baker, M. Roy, D. Peddis, J.Phys: Condensed Matter 22 (2010) 436005.
[39] E.P. Yelsukov, E.V. Voronina, V.A. Barinov, J. Magn. Magn. Mater. 115 (1992) 271.
[40] E.M. Chudnovsky, J. Magn. Magn. Mater. 40 (1983) 21.
[41] E.M. Chudnovsky, W.M. Saslow, R. Serota, Phys. Rev. B 33 (1986) 251.
[42] W.M. Saslow, Phys. Rev. B 35 (1987) 3454.
[43] C. Binns, M.J. Maher, New J. Phys. 4 (2002) 85.
[44] C. Binns, M.J. Maher, Q.A. Pankhurst, D. Kechrakos, K.N. Trohidou, Phys. Rev. B 66 (2002) 184413.
[45] J.F. Löffler, J.P. Meier, B. Doudin, J.P. Ansermet, W. Wagner, Phys. Rev. B 57 (1998) 2915.
[46] J.F. Löffler, H.B. Braun, W. Wagner, Phys. Rev. Lett. 85 (2000) 1990.
[47] E.M. Chudnovsky, in: F. Baca, W.Y. Ching (Eds.), The Magnetism of Amorphous Metals and Alloys, 1995 ch 3.
[48] M.T. Qureshi, Nanostructured Magnetic Films Produced by Magnetic Nanoparticles, PhD thesis, 2012.
[49] E.M. Chudnovsky, J. Appl. Phys. 64 (1988) 5770.
[50] M.S. Kurt, S.H. Baker, M. Roy, M.R. Lees, J. Magn. Magn. Mater. 471 (2019) 549.